JCIM JOURNAL OF CHEMICAL INFORMATION AND MODELING

pubs.acs.org/jcim Article

Benchmarking Cofolding Methods for Molecular Glue Ternary Structure Prediction

Yiyan Liao,[#] Jintao Zhu,[*,#] Juan Xie, Luhua Lai,[*] and Jianfeng Pei[*]

Cite This: https://doi.org/10.1021/acs.jcim.5c01860 Read Online

ACCESS | Metrics & More | Article Recommendations | Supporting Information

ABSTRACT: Molecular glues (MGs) represent an emerging therapeutic paradigm capable of inducing or stabilizing protein−protein interactions (PPIs), with broad applications in creating neomorphic interactomes and targeted protein degradation. However, current discovery efforts remain largely confined to experimental screening, while *in silico* rational design of MGs remains a formidable challenge. A critical step toward rational design lies in accurate ternary complex modeling, which is less explored and highly challenging due to the involvement of small-molecule-induced *de novo* PPIs. Here, we tested the ability of recently developed cofolding models, including AlphaFold 3, Boltz-1, Chai-1, Protenix, and RoseTTAFold All-Atom. Although these models were not specifically trained on ternary complex structures, whether their capability to learn diverse interatomic interactions can generalize well to such ternary systems remains an open question. We systematically curated a data set, named MG-PDB, with 221 noncovalent MG-engaged ternary complexes. MGBench was further introduced as a comprehensive benchmark set, which comprises 88 ternary structures excluded from cofolding models' training data through rigorous time-based partitioning. Our benchmark results demonstrated that AlphaFold 3 achieved the best overall performance among cofolding methods, in terms of both PPI interface prediction (50.6% success rate) and MG−protein interaction recovery (32.9% success rate). However, our homology study showed that most of their successful predictions actually stemmed from memorization. Further analysis revealed three phenomena of current cofolding methods for MG ternary structure prediction. First, these methods struggle to accurately model large interaction interfaces. Second, their predictive accuracy is notably reduced for domain−domain complexes compared to domain−motif interactions. Lastly, they face specific challenges in modeling MG degrader complexes with sufficient accuracy. We showcased they relied on the existing interaction patterns and highlighted the need for further improvements in novel E3 ligase systems. These findings reveal fundamental gaps in existing methods to learn atomic-level interaction rules for MG-engaged ternary complex modeling. As fully open resources, MG-PDB and MGBench establish the essential benchmark for MG ternary complex modeling, providing the definitive standard for evaluating future cofolding methods.

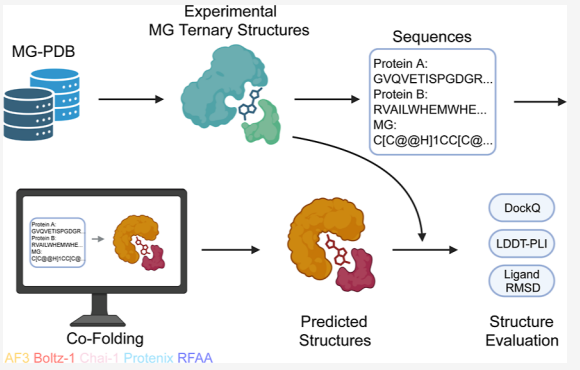

INTRODUCTION

Chemically induced proximity has emerged as an attractive strategy in modern drug discovery, with broad biological applications in modulating protein−protein interactions (PPIs), including creating neomorphic PPIs[1] and targeted protein degradation (TPD).[2−4] As a central paradigm of such strategy, molecular glues (MGs) have, since their discovery more than 30 years ago,[5−7] garnered significant attention. Interest in their design was particularly spurred by the discovery in 2000 that a simple synthetic compound, syntab-A, could induce associations of native proteins.[8] This design paradigm has since proven particularly valuable in degrader development, due to the favorable drug-like properties of MGs.[9−12] Consequently, MGs have achieved notable clinical success, with at least nine FDA-approved drugs functioning as MGs.[13] Notably, MGs provide access to challenging targets such as transcription factors[14,15] and intrinsically disordered proteins[16] that are traditionally considered undruggable. Mechanistically, MGs typically refer to monovalent small molecules[17,18] (with the exception of a few natural products) that either induce neomorphic PPIs or stabilize native PPIs by cooperatively binding at a PPI interface.[19−21]

Based on the mechanism of action (MOA) and downstream biological effects, MGs can be classified into three categories: molecular glue degraders (MGDs), nondegradative heterodimerizing MGs, and homodimerizing MGs.[17] MGDs represent a special class of MGs that induce the binding of target proteins to E3 ubiquitin ligases, thereby triggering

Received: August 5, 2025
Revised: October 2, 2025
Accepted: October 3, 2025

ubiquitination and subsequent proteasomal degradation of the target proteins.[19] Nondegradative heterodimerizing MGs, on the other hand, modulate protein function without degradation by inducing or enhancing native PPIs.[12] Homodimerizing MGs (self-association MGs) promote protein self-association, leading to the formation of higher-order assembly, which may alter the native state of proteins and influence their function.[22,23] Despite the diversity in their MOA, all MGs mediate the formation of ternary complexes with two protein partners, which serves as the molecular basis for exerting broad regulatory effects on cellular functions.

A key advantage of MGs over bivalent molecules such as proteolysis-targeting chimeras (PROTACs) is their superior physicochemical properties. MGs typically have lower molecular weights, allowing them to maintain compliance with established drug-likeness guidelines, such as Lipinski's rule of five, which are considered critical for achieving oral bioavailability.[24] However, a number of rational design approaches[25−28] have been developed to accelerate the design of PROTACs. These heterobifunctional molecules are composed of a warhead binding to a protein of interest (POI), an E3 ligase ligand, and a linker that connects the two moieties.[29] As many E3 ligase ligands and POI warheads are well characterized, the rational design of PROTACs typically centers on the optimization of the linker.[30] In contrast, the rational design of MGs is a more formidable challenge due to the structural complexity and dynamics of ternary structures.

In the past decade, MG discovery has mainly relied on experimental screening and following optimization.[31] For example, the thalidomide and lenalidomide were identified as MGD years after their clinical use.[4,32−34] Traditional experimental screening methods for discovering MGs can be primarily divided into activity-based (ABMs) and interaction-based approaches (IBMs).[13] ABMs evaluate the effects of molecules by measuring downstream activities in cells or *in vitro*. For instance, cyclin K degraders dCeMM2-4 were discovered by screening a small-molecule library for compounds with E3-dependent antiproliferative activity.[35] IBMs directly measure the interactions between two proteins upon the addition of molecules. RO-2443 was discovered by screening molecules for suppression of p53-MDMX binding using the TR-FRET assay.[36] However, these methods typically require large-scale, high-cost experimental platforms. To accelerate the discovery of MGs and reduce costs, computational approaches for screening and rational design of MGs must be developed.

With the advancement of computer-aided drug design, structure-based drug design could be considered for MG discovery, enabling the exploration of a broader chemical space for effective MGs or neosubstrates.[37] The structural modeling of MG-engaged ternary complexes is of significant importance for structure-based MG screening and design. Notably, any binary combination of the ternary components typically exhibits low or undetectable binding affinity, and before engagement, well-defined binding pockets are not a prerequisite for complex assembly.[38] Such a cooperative binding mechanism with concurrent pocket formation necessitates modeling approaches that accommodate extensive conformational rearrangements in MG-engaged ternary complexes, exceeding the current capabilities of conventional induced-fit docking[39] and AI-based flexible docking methods.[40,41] Furthermore, this induced nature of the interaction implies that coevolutionary signals, a key source of information for predicting naturally evolved protein complexes,[42] cannot contain useful information as the two proteins have never evolved to form a complex. Recently, AI technology has achieved groundbreaking progress in biomolecular structure prediction. AI cofolding methods[43−47] have been introduced to learn general molecular interactions and predict various biomolecular complex structures. RoseTTAFold All-Atom (RFAA)[43] was the first to achieve a unified representation of multiple biomolecular types; AlphaFold 3 (AF3)[44] introduced a diffusion module on the basis of its previous version AF2,[48] enabling atomic-level structure prediction. Subsequent models, including Chai-1,[45] Boltz-1,[46] and Protenix,[47] have replicated and improved upon AF3, achieving similar structure prediction capabilities. These cofolding methods perform *de novo* structure modeling from protein sequence and molecular format in SMILES, rendering them particularly suited for *in silico* determination of MG-engaged ternary complexes.

Cofolding methods have been benchmarked in several applications, including protein−ligand cofolding,[49] protein−protein complexes,[50] G protein-coupled receptor−ligand systems,[51] and PROTAC-mediated ternary complexes.[52] While demonstrating considerable modeling accuracy, these methods still rely heavily on memorization of training data[49] and often exhibit significant errors, limiting their capability for high-precision interaction prediction. Their application to MG ternary structure modeling remains unexplored, presenting both a critical test of model generalizability and an opportunity to guide future methodological development of this emerging therapeutic paradigm.

In this work, we aim to evaluate the performance of the cofolding approach in modeling MG ternary complex structures. This effort serves as a foundation for enabling the structure-based rational design of MGs, thereby facilitating future structure-based virtual screening and *de novo* design of MGs. Here, we carefully establish a data set consisting of 221 noncovalent MG-engaged ternary complexes, named MG-PDB. Due to the lack of relevant benchmark sets, we further introduce MGBench from MG-PDB for comprehensive evaluation of MG-engaged ternary structure prediction, which includes 88 ternary structures released after cofolding method training. We then present a comparative assessment of five state-of-the-art (SOTA) cofolding methods (AF3, Boltz-1, Chai-1, Protenix, and RFAA) across MGBench. Our benchmark analysis reveals that AF3 outperforms other cofolding methods, achieving relatively better prediction accuracy for PPI interfaces and recovery rate for MG−protein interactions. However, we observe that the memorization effect contributes significantly to this performance. Through systematic evaluation of structural determinants and mechanistic case studies, we identify critical limitations in modeling large interacting interfaces, domain−domain complexes, and degradation-specific glue mechanisms. These findings establish essential quality baselines while highlighting fundamental gaps in current approaches' ability to capture ternary-molecule interactions. Our work provides comprehensive data resources, quantitative performance metrics, and mechanistic insights to guide future development of structure prediction tools for MG discovery.

METHODS

Data Collection. We conducted a systematic search of complex structures on PDB[53,54] using MG-related keywords, collecting and annotating all the structures, with detailed

https://doi.org/10.1021/acs.jcim.5c01860
J. Chem. Inf. Model. XXXX, XXX, XXX−XXX

information listed in Supporting Information (XLSX file). Specifically, each entry was manually validated as an authentic MG ternary complex based on three key criteria: (1) structural confirmation of the small molecule's position at the PPI interface; (2) explicit description in the primary literature using terms such as "molecular glue", "molecular glue degrader", or "PPI stabilizer"; and (3) the presence of supporting experimental data, such as surface plasmon resonance (SPR) and isothermal titration calorimetry (ITC), that demonstrates molecule-induced complex formation. We manually downloaded the mmCIF files and fetched structural-related information through RCSB PDB Data API.[55] To facilitate analysis of protein pairs directly interacting with MGs, we systematically annotated the two protein chain identifiers that establish direct interactions with the MG in each PDB entry as well as the CCD code of MGs. All entries were rigorously validated as authentic MG complexes and annotated with MOA class through original literature, ensuring data set reliability for downstream benchmarking. Notably, this study exclusively focuses on noncovalent MG-induced ternary complexes. For each PDB entry, we programmatically retrieved directly interacting protein partners' sequences through the RCSB PDB Data API[55] while manually curating canonical SMILES representations of MGs—both serving as foundational input for structural reconstruction workflows. Following the category rule established by Rui et al.,[56] we further categorized and annotated the collected complex structures into two distinct domain types: (1) domain−domain: characterized by interactions between well-structured protein domains and (2) domain−motif: defined by one of the binding partners being a short linear motif containing a specific recognition sequence.

MGBench Curation. For the 221 ternary complex PDB structures we collected, we first removed structures determined by X-ray diffraction (XRD) with a resolution worse than 3.5 Å. For electron microscopy (EM) structures, we further examined the local resolution representations at the MG-binding interface; if the interface resolution met the 3.5 Å criteria, the structure was retained even if the overall resolution was lower than 3.5 Å. We further retained structures with a release date after 2021-09-30 as MGBench including 88 structures, excluding structures used in the training sets of the methods. To further investigate the impact of sequence homology between MGBench and cofolding methods' training data, we extracted sequences from all PDB structures released before 2021-09-30 as training data and performed a similarity search using MMSeqs2[57] on all sequences in MGBench. Following AF3's approach for evaluating interface metrics,[44] we applied the following filtering criteria:

- If both polymers have a length of at least 16 amino acids and exhibit greater than 40% sequence identity to two chains in the same complex in the training data, the structure is filtered out.
- For structures containing chains with fewer than 16 residues, the similarity of the longer chain must be less than 40% sequence identity to any structure in the training data.

Finally, we retained 25 structures as the MGBench low-homology set, while the remaining 63 structures were designated as the MGBench high-homology set.

Given the significant quality variance among different structures, we conducted a structural quality performance analysis of the MGBench. Following the previously established criteria for high-quality structures,[58,59] we adopted the following standards. The global quality filters required a resolution of ≤2.5 Å; a diffraction precision index (DPI) of ≤0.42;[60] an *R*-factor of ≤0.20; an *R*-free of ≤0.25; and passing of the overfitting test (difference between the *R*-factor and *R*-free ≤0.05). The local MG quality filters required passing of the crystal contacts test (no crystal symmetry contacts in the active site); an occupancy-weighted average *B*-factor (OWAB) of ≤50 Å^2; a maximum atomic ligand *B*-factor of ≤50 Å^2; and a ligand real-space *R* correlation coefficient (RSCC) of ≥0.8.[61] All metrics were calculated using the StructureProfiler tool.[59] Ultimately, we retained 23 structures as the MGBench high-quality (HQ) set, while the remaining 65 structures were designated as the low-quality (LQ) MGBench set.

Ternary Structure Prediction. We evaluated five SOTA cofolding methods for MG ternary complex reconstruction: AF3,[44] Chai-1[45] (https://lab.chaidiscovery.com/), Boltz-1,[46] Protenix[47] (https://protenix-server.com), and RFAA.[43] A summary of the different methods is provided in the Supporting Information Methods. To ensure a rigorous evaluation of their maximum predictive performance, all methods were implemented under optimal configurations, including the use of multiple sequence alignments and default parameter settings. For Chai-1 and Protenix, predictions were generated via their real-time updated web servers to leverage the most current implementations. The remaining methods (AF3, Boltz-1, and RFAA) were run locally by using the latest software versions. Structural visualization and comparative analysis were performed using ChimeraX-1.9.[62]

Ternary Structure Evaluation. We systematically evaluated reconstruction accuracy through comparative analysis between the predicted models and experimentally determined PDB structures. Despite inherent experimental uncertainties of PDB structures, depending on factors such as resolution and *R*-factor, we still use them as our gold standard, following the established evaluation strategy of models like AF3.[44] The assessment employed three established metrics: (1) DockQ score for protein−protein interface quality assessment,[63] (2) LDDT-PLI (local distance difference test for protein−ligand interactions) to assess the recall of contacts between ligands and pockets, and (3) ligand RMSD to measure the accuracy of ligand-binding pose prediction based on binding-site superposition.[64] Specifically, the formulas for the three metrics are defined as follows:

$$\text{DockQ} = \frac{1}{3}\left(f_{\text{nat}} + \frac{1}{1+\left(\frac{\text{iRMSD}}{1.5}\right)^2} + \frac{1}{1+\left(\frac{\text{LRMSD}}{8.5}\right)^2}\right) \tag{1}$$

Here, f_{nat} quantifies the fraction of correctly predicted interfacial contacts, iRMSD measures structural divergence at the binding interface using backbone atom RMSD, and LRMSD evaluates global structural alignment by computing the backbone deviation between predicted and native structures after optimal superposition.

$$\text{LDDT-PLI} = \frac{1}{4N}\sum_{i=1}^{N}\sum_{k=1}^{4} I(|d_{\text{pred}}^{(i)} - d_{\text{ref}}^{(i)}| \le t_k) \tag{2}$$

Here, N represents the number of effective atom pairs within the inclusion radius (here, 6.0 Å) between ligand atoms and

https://doi.org/10.1021/acs.jcim.5c01860
J. Chem. Inf. Model. XXXX, XXX, XXX−XXX

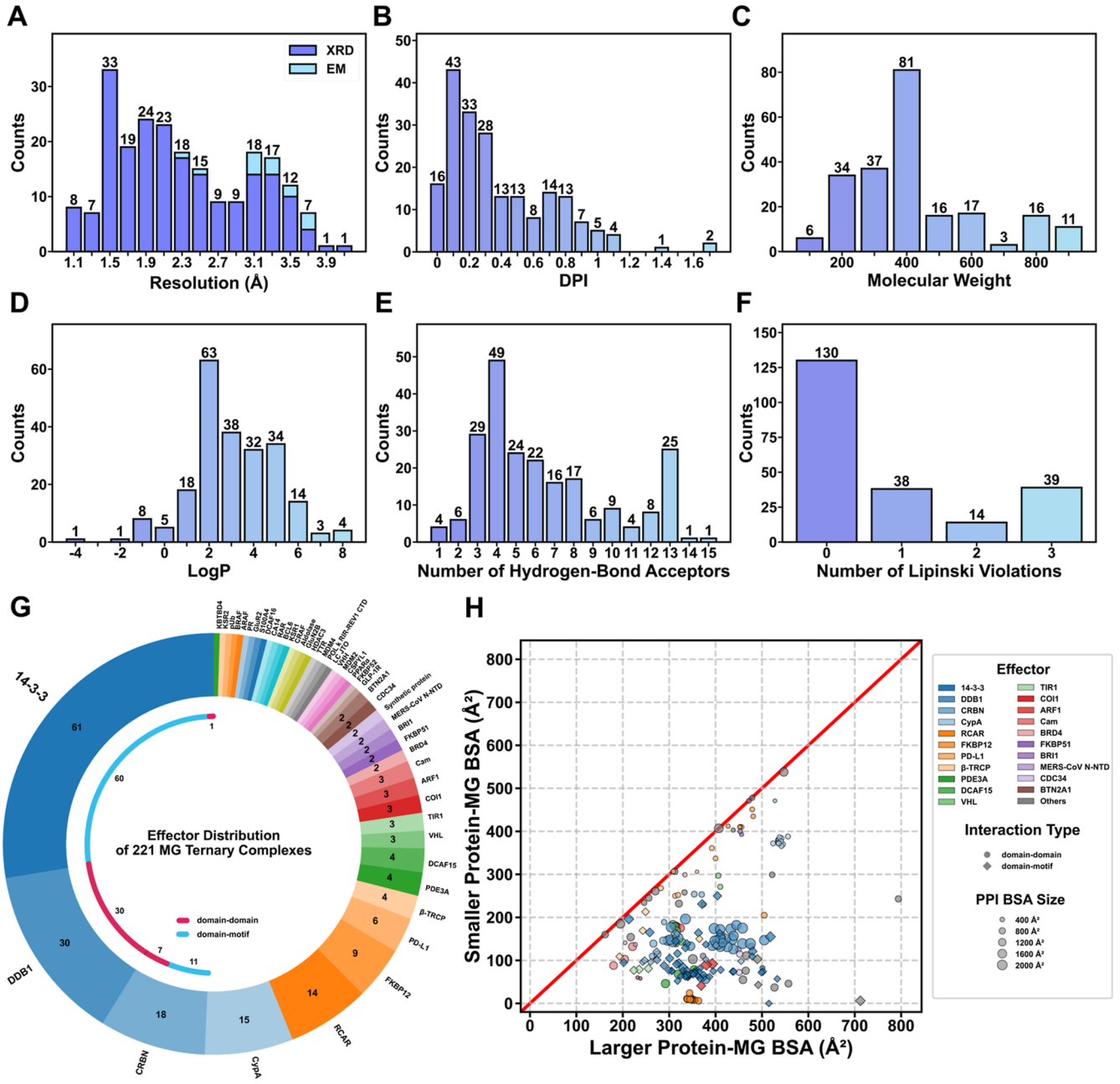

Figure 1. Overview of MG-PDB. For structure qualities, distribution plots showing distribution of resolution (A) and DPI (B) for all crystal structures (DPI is not available for certain cases). For MG molecular properties, distribution plots showing distribution of heavy molecular weight (C) and log *P* (D), and histograms showing number of hydrogen-bond acceptors (E) and number of Lipinski violations (F). In plots (A–D), each bar represents a bin interval starting at the labeled value (i.e., $[x, x + \text{width})$), while in (E,F), each bar represents a discrete value. Doughnut chart showing the classification of the MG ternary complexes by the effector protein (G). The inner circle provides a detailed breakdown of interacting modes for complexes involving 14–3–3, DDB1, or CRBN. Scatter plot showing the BSA distribution of MG ternary complexes (H). Scatters are colored by effector proteins, with the shape indicating which interacting mode the complex belongs to (domain–domain: circle, domain–motif: diamond) and symbol size indicating PPI BSA of the ternary complex. XRD: X-ray diffraction; EM: electron microscopy.

surrounding protein atoms in the reference structure. $d^{(i)}_{\text{pred}}$ denotes the distance between the *i*-th ligand–pocket atom pair in the predicted structure, $d^{(i)}_{\text{ref}}$ is the corresponding atomic pair distance in the reference structure, t_k is the preset threshold (here 0.5, 1.0, 2.0, and 4.0 Å), and $I(\theta)$ is the indicator function.

$$\text{Ligand RMSD} = \sqrt{\frac{1}{n}\sum_{i=1}^{n}(x_i - y_i)^2} \tag{3}$$

Here, n represents the number of heavy atoms in the ligand, x_i denotes the coordinate of the *i*-th atom in the ligand for the predicted conformation, and y_i signifies the coordinate of the *i*-th atom in the ligand for the ground truth conformation. To calculate the ligand RMSD, the binding sites were first aligned by superposing all protein residues within 4 Å radius of the ligand.

Computational workflows were implemented by using specialized tools: DockQ calculations utilized the official DockQ package,[63] while LDDT-PLI and ligand RMSD metrics

https://doi.org/10.1021/acs.jcim.5c01860
J. Chem. Inf. Model. XXXX, XXX, XXX−XXX

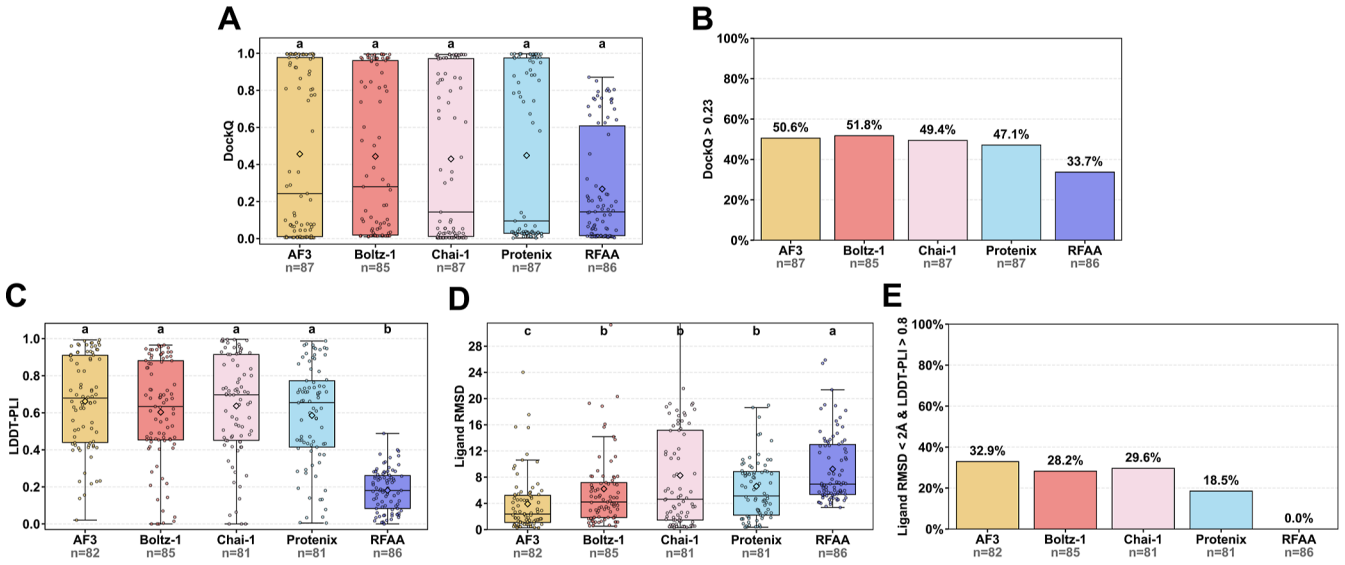

Figure 2. Overall metrics distributions of structural modeling in MGBench. For PPI interfaces, the box plot depicts the DockQ distribution (A) and the histogram shows the success rate defined by DockQ >0.23 (B) for structures reconstructed by cofolding methods. For ligand-pocket binding conformations, box plots depict LDDT-PLI (C) and ligand RMSD (D) distributions, and the histogram shows the success rate defined by ligand RMSD <2 Å combined with LDDT-PLI >0.8 (E) for structures generated by cofolding approaches. *n* represents the number of successfully modeled structures for each method. In box plots, the diamond symbol represents the mean value, and different letters indicate significant differences.

were computed through OpenStructure's built-in validation toolkit.[65]

Calculation of the BSA. The BSA was determined by utilizing ChimeraX-1.9.[62] All solvent molecules, ligands other than MGs, and irrelevant protein chains were removed. Unique sequence identifiers were assigned to the ligands, distinct from those of the proteins. The "interfaces" command was then employed to calculate BSA for each pair of interacting chains within the complexes. We proceeded with further analysis using the BSA values obtained from PPIs.

RESULTS

Systematic Collection and Analysis of Experimental MG Ternary Structures. To evaluate the reconstruction capability of various cofolding methods for MG ternary complexes, we collected MG-related structures from the Protein Data Bank (PDB) database. We manually reviewed the annotated CCD IDs of MG and the protein chain identifiers directly interacting with MG, and we further determined the MOAs through original literature sources. In total, we obtained 221 noncovalent MG-engaged ternary complexes, named MG-PDB, comprising 207 structures determined by X-ray diffraction and 14 structures determined by electron microscopy. A detailed analysis of MG-PDB was conducted to ensure its representativeness and high quality. Based on the classification of MOA, MG-PDB encompasses 67 MGDs, 134 nondegradative heterodimerizing MGs, and 20 homodimerizing MGs. Additionally, following the previous study,[56] 221 ternary complex structures are classified into 136 domain−domain structures and 85 domain−motif structures based on the two protein-binding partners (Table S1). Detailed statistical analysis shows 91.0% (200/221) of structures have resolutions below 3.5 Å and 62.9% (139/221) below 2.5 Å (Figure 1A). 61.5% (123/200, not available for certain cases when calculated with StructureProfiler[59]) of diffraction precision index (DPI) values are below 0.42 (Figure 1B).[60] These results indicate that the data set includes low-resolution structures, highlighting the need for our downstream analysis to consider the impact of structural quality. Analysis of MG property distributions further demonstrates broad coverage of drug-like molecules within MG-PDB (Figure 1C−F), mostly conforming to the characteristic features of MGs.[10] Furthermore, we assessed the number of violations to Lipinski's rule of five, revealing that approximately 60% of MGs fully comply with the rule (Figure 1F).

A detailed analysis of the effectors involved in the ternary complexes was conducted (Figure 1G). There are a total of 48 effector proteins in MG-PDB (excluding synthetic proteins), representing more than double the diversity reported in previous studies.[56] Among these, 14−3−3/nondegradative heterodimerizing MGs, DDB1/MGDs, and CRBN/MGDs in sum account for nearly half of the whole benchmark, reflecting the current landscape of research in the MG field. Notably, most of the ternary complexes mediated by 14−3−3 or CRBN belong to the domain−motif type. Buried surface area (BSA) quantifies the extent of surface area buried upon complex formation and typically indicates the complexity of intermolecular interactions, potentially correlating with binding affinity.[56,66] We analyzed the PPI BSA as well as the two protein−MG BSAs across all of the ternary complexes (Figure 1H), revealing considerable diversity. The PPI BSA ranges from a minimum of 190 Å^2 to a maximum of 2400 Å^2, spanning a wide range. For the protein−MG BSAs, consistent with prior observations,[56] the majority of compounds exhibit asymmetric binding, where MG buries a larger surface area with one protein compared to the other. And domain−motif-type complexes display a more pronounced asymmetric binding pattern as expected. Collectively, our benchmark demonstrates broad representativeness, diversity, and reliability, making it well suited for benchmarking cofolding approaches.

A Standard Benchmark for MG Ternary Structure Modeling. To ensure the high quality of structure, we first

https://doi.org/10.1021/acs.jcim.5c01860
J. Chem. Inf. Model. XXXX, XXX, XXX−XXX

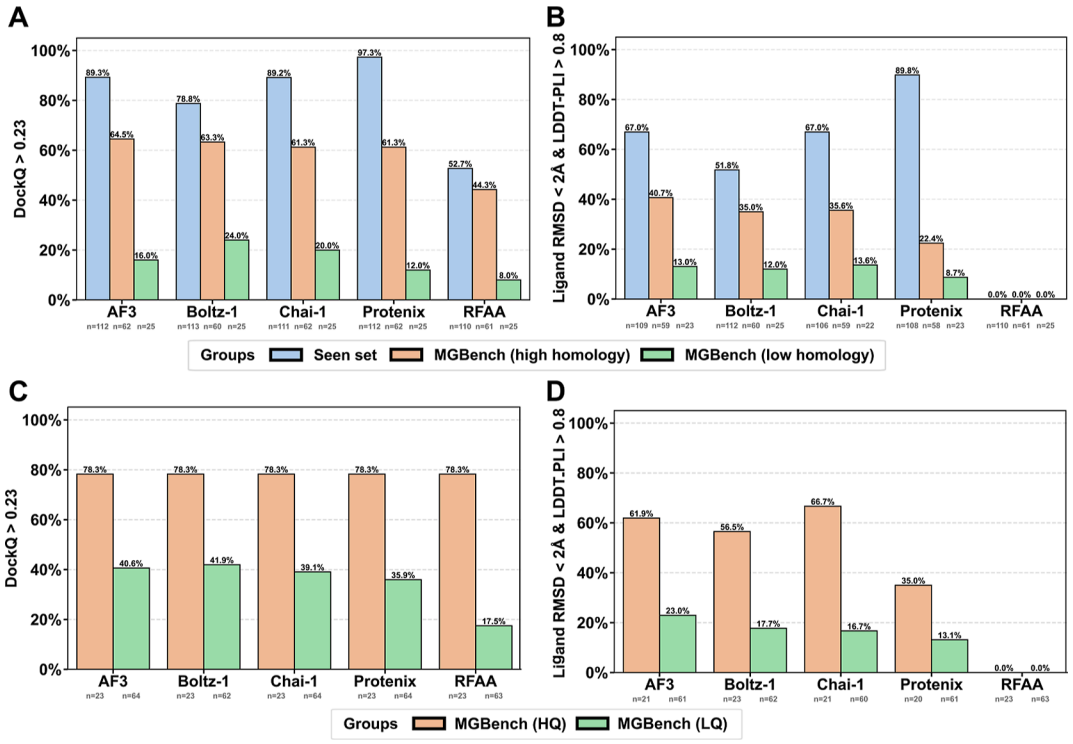

Figure 3. Homology and quality analysis among cofolding methods. Histograms showing the acceptable rates of PPI interface quality (A,C) and recovery rate of native ligand−pocket interaction (B,D) on the seen set (i.e., structures in resolution-filtered MG-PDB but not in MGBench), MGBench high-homology set, MGBench low-homology set, MGBench HQ set, and MGBench LQ set. *n* represents the number of successfully modeled structures for each group.

performed a structural quality filtering on the MG-PDB data set. Structures determined by X-ray diffraction with a resolution of worse than 3.5 Å were removed. For electron microscopy structures, we further examined the local resolution representations at the MG-binding interface; if the interface resolution met the 3.5 Å criteria, the structure was retained even if the overall resolution was lower than 3.5 Å. This filtering process resulted in the retention of 202 structures, and this resolution-filtered MG-PDB data set was used to perform subsequent analyses. To assess the generalization capabilities of cofolding methods, we constructed a standard benchmark utilizing structures released after 2021-09-30, called MGBench (88 structures in total). This temporal partitioning reflects evolving trends in scientific advancement and has been adopted by multiple AF3 benchmark works.[49,51,52,67] Following the interface metrics criteria for the evaluation set in AF3[44] (as detailed in the Methods section), we performed additional homology filtering on MGBench, resulting in a final selection of 25 ternary complex structures designated as the MGBench low-homology set. The remaining 63 structures were classified as the MGBench high-homology set. Furthermore, to investigate the effect of structural quality on modeling precision, we performed a structure quality split based on a series of criteria (detailed in the Methods section). This process yielded a high-quality (HQ) set comprising 23 ternary complexes and a low-quality (LQ) set of the remaining 65, designated as the MGBench HQ and MGBench LQ sets, respectively.

Overall Evaluation on MGBench. Then, we performed ternary structure predictions using five cofolding methods, i.e., AF3, Boltz-1, Chai-1, Protenix, and RFAA on both resolution-filtered MG-PDB and MGBench. The number of successfully predicted structures for each method is presented in Table S2. The small number of failures can be attributed to two main categories of technical issues: (i) prediction failures, stemming from computational constraints such as GPU memory limits or errors in ligand conformer generation, and (ii) evaluation failures, where the predicted ligand could not be matched to the native structure via subgraph isomorphism in OpenStructure. Since these few technical failures are nonsystematic and rare, their exclusion has a negligible statistical impact on the overall conclusions.

We conducted a comprehensive assessment of the structural quality of ternary complex reconstructions using different methods. The quality of PPI interfaces was evaluated using DockQ (Figures 2A,B and S1A,B). The DockQ distributions, except for RFAA, exhibited a similar bimodal distribution (Figures 2A and S1A), indicating that the majority of structures had either high DockQ scores (greater than 0.8) or very low scores (less than 0.1). Generally, structures with a DockQ greater than 0.23 are considered acceptable.[44,68] Except for RFAA, the success rate of modeling acceptable PPI interfaces on resolution-filtered MG-PDB was approximately 70% (Figure S1B), while it dropped to around 50% for MGBench structures (Figure 2B), suggesting a limited generalization capability in reconstructing PPI interfaces. The performance of RFAA was significantly inferior to other methods, and its insufficient ability to avoid intermolecular collisions was observed.

LDDT-PLI is used to evaluate atomic-level local distance deviations at protein−ligand interaction interfaces, measuring the ability of the reconstructed models to recapitulate MG-protein binding modes. Studies indicate that LDDT-PLI >0.8 is thought to reflect a reliable interaction mode.[64] The LDDT-

https://doi.org/10.1021/acs.jcim.5c01860
J. Chem. Inf. Model. XXXX, XXX, XXX−XXX

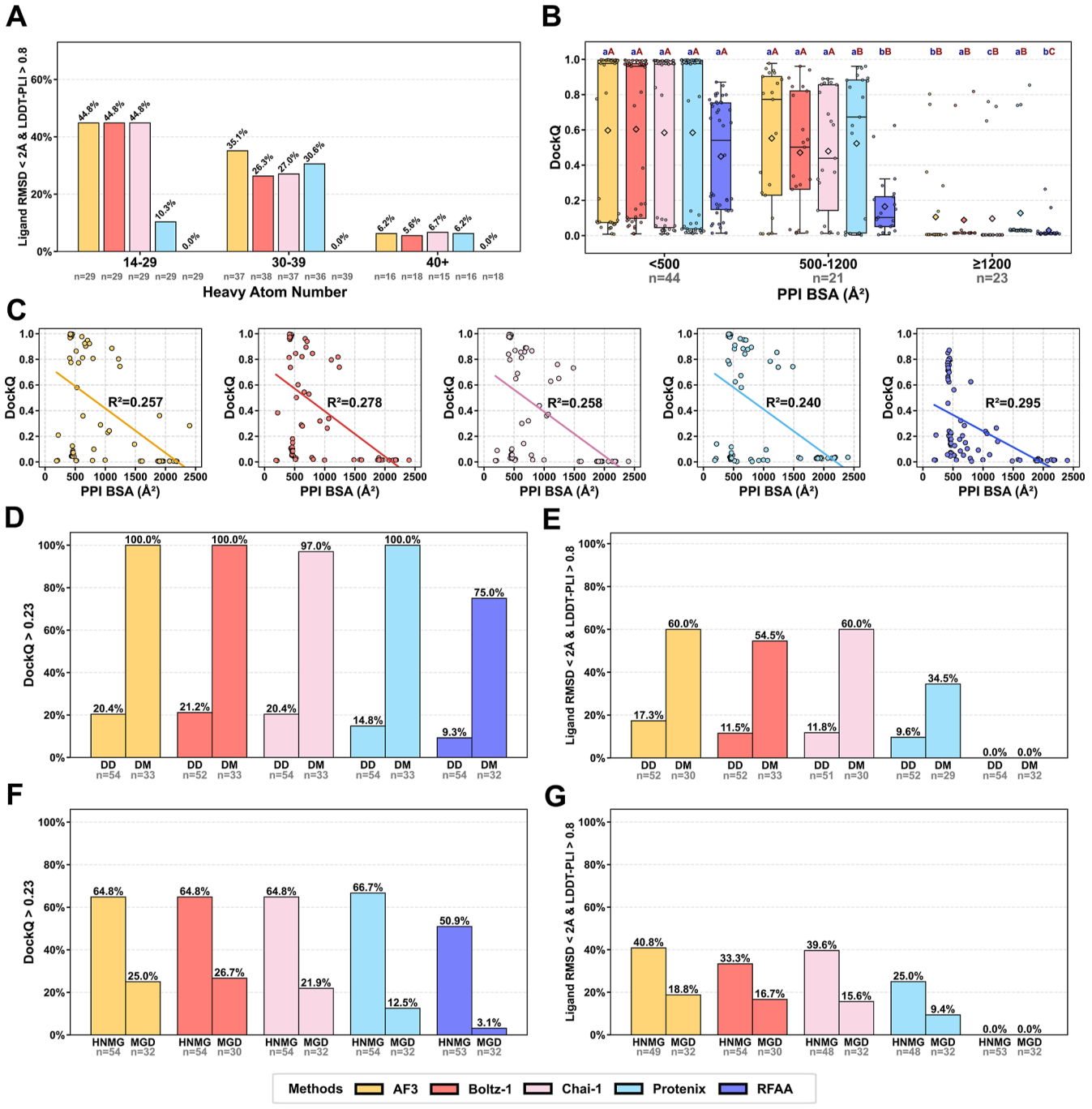

Figure 4. Analysis of key factors influencing MG-engaged ternary complex prediction. Histogram showing the success rate across the heavy atom number for reconstructed structures from MGBench (A). Box plot showing the distribution of DockQ categorized based on the BSA of native ternary complex structures (<500 Å^2, 500−1200 Å^2, >1200 Å^2) (B), and scatter plots displaying the relationship between DockQ and BSA of native structures, along with the fitted regression line (C). Histograms showing the impact of interacting mode (DD: domain−domain, DM: domain−motif) on the PPI interface quality (D) and recovery of native ligand−pocket interaction (E). Histograms showing the impact of the MG type (HNMG: nondegradative heterodimerizing MG, MGD: MG degrader) on the PPI interface quality (F) and recovery of native ligand−pocket interaction (G). In the box plot, the diamond symbols represent the mean value, with lowercase letters indicating significance between different methods (same BSA group) and uppercase letters indicating significance between different BSA groups (same method). *n* represents the number of successfully modeled structures for each group.

PLI distribution results show that for resolution-filtered MG-PDB structures, the median values of all methods (except RFAA) are around 0.8 (Figure S1C), whereas for MGBench structures, they all fall below 0.7 (Figure 2C), indicating insufficient accuracy. Ligand RMSD assesses the precision of MG binding pose prediction. A ligand RMSD <2 Å is generally considered indicative of native-like conformations. Results demonstrate that while the median RMSD for resolution-filtered MG-PDB structures is around this threshold (Figure S1D), performance degrades significantly for MGBench structures (Figure 2D), there is room for improvement to reproduce ligand-binding poses. Notably, AF3 achieves

https://doi.org/10.1021/acs.jcim.5c01860
J. Chem. Inf. Model. XXXX, XXX, XXX−XXX

significantly lower Ligand RMSD values than other methods, highlighting its superior accuracy in predicting MG-binding poses.

Based on the previously established criteria for AI-based protein−ligand cofolding structure prediction,[49] we evaluated the success rates of different models in the recovery of native ligand−pocket interaction using the dual criteria of ligand RMSD <2 Å and LDDT-PLI >0.8. As shown in Figures 2E and S1E, the performance varied significantly among the models. RFAA failed to generate any successful predictions, indicating its lower accuracy. Compared to the success rates of approximately 50% for resolution-filtered MG-PDB structures, the success rates of all models dropped to approximately 30% for MGBench structures, suggesting limited capability of these methods for native ligand−pocket interaction reconstruction. Notably, AF3 demonstrated the highest success rate (32.9%) among all models for MGBench structures, indicating its relatively stronger performance.

We further conducted a sequence homology analysis on MGBench, examining the reconstruction success rates on both the MGBench high-homology set and MGBench low-homology set (Figure 3A,B). A clear observation was that the structural reconstruction success rate on the MGBench low-homology set was significantly lower than that on the MGBench high-homology set, indicating a memorization effect across the methods. This finding aligns with conclusions from previous benchmarking.[49]

As reliable evaluation results must be obtained on high-quality structures, we further split MGBench into a HQ subset and an LQ subset based on stringent structural quality criteria (see details in the "MGBench Curation" subsection). We found that the success rate was significantly higher in the MGBench HQ set than in the MGBench LQ set (Figure 3C,D). This remarkable improvement in performance underscores the critical influence of the structure quality. On the HQ subset, all cofolding methods demonstrated comparable accuracy in modeling acceptable PPI interfaces, while AF3 maintained a leading performance in modeling MG−protein interactions.

Analysis of Key Factors Influencing MG-Engaged Ternary Complex Prediction. In the preceding section, we observed significant variability in the reconstruction performance across different ternary complex structures, suggesting that intrinsic structural properties strongly influence the outcomes. To further evaluate the impact of distinct structural features on the assessment metrics, we conducted a detailed subgroup analysis based on the following parameters: (1) the number of heavy atoms in the MG, (2) BSA of the PPI interface, (3) protein interacting mode (domain−domain/domain−motif), and (4) the downstream functional type of the MG (MGDs/nondegradative heterodimerizing MGs/homodimerizing MGs).

First, to assess the model's reconstruction capability for MGs with the heavy atom number, we analyzed success rates in the recovery of native ligand−pocket interaction as a function of heavy atom number (Figure 4A). The overall trend revealed a notable decline in prediction accuracy for MGs with larger MG molecules, indicating potential limitations in the training set's coverage and insufficient learning of chemical space. Specifically, MGs with a large heavy atom number are often natural products, whose structural diversity and conformational complexity may introduce prediction challenges.[69,70]

The BSA of the PPI interfaces typically reflects the size of the PPI interface. Previous studies have attempted to explore the correlation between BSA and binding affinity data in MG ternary complexes.[56] Here, we calculated the BSA of native MG ternary complexes and analyzed its relationship with the DockQ metric (Figure 4B−C). Within MGBench, a clear negative correlation between BSA and DockQ was observed (Figure 4B), indicating that current methods struggle to accurately model large PPI interfaces. Linear regression analysis between DockQ and BSA further confirmed this negative correlation with all methods showing correlation coefficients of more than 0.25 (Figure 4C), reinforcing our conclusion. In summary, current cofolding methods fail to adequately model the PPI mechanisms in MG-engaged ternary complexes, and their modeling quality deteriorates significantly as the PPI interface size increases.

We investigated the impact of protein interacting mode categories on the evaluation metrics. The results (Figures 4D−E and S2) demonstrate significant differences in all metrics between domain−domain and domain−motif groups across all methods, indicating that the reconstruction quality of domain−motif structures is significantly higher than that of domain−domain structures. Notably, the success rate (DockQ >0.23) for MGBench-reconstructed structures approaches 100% in all methods (except RFAA) (Figure 4D), which aligns with our previous conclusion since domain−motif structures typically feature smaller PPI interfaces and BSA. Furthermore, the native interaction recovery also shows significantly higher success rates for domain−motif structures (Figure 4E). The achieved performance is not surprising, as nearly all domain−motif structures in MGBench exhibit high homology to those in the training set, where only CRBN and 14−3−3 hub protein-mediated ternary complex systems were included (Table S3).

To support the design of MGs with different MOAs, we separately analyzed the distribution of the reconstruction metrics. The results show that the quality of reconstructed ternary complexes induced by MGDs is significantly poorer across multiple metrics (Figures 4F−G and S3), achieving only ∼20% DockQ success rate and ∼15% native interaction recovery rate on MGBench, respectively (Figure 4F−G). Currently, research and design of MGs primarily focus on MGDs utilizing TPD mechanisms. Here, we emphasize that current cofolding methods fail to meet the precision requirements for modeling MGD-engaged structures, making it challenging to elucidate the mechanisms of MGDs and *in silico* design.

Case Studies for Structural Modeling of Ternary Complexes between MGD-Engaged E3 Ligase and Neosubstrate. We selected representative structures from the MGBench low-homology set for a detailed analysis. The WIZ zinc finger protein associates with the cohesin/CTCF complex at DNA loops involved in regulating gene expression and genome architecture[71,72] and has been linked to the pathogenesis of sickle cell disease.[15] Recently, Novartis Biomedical Research reported the development of dWIZ-1, a thalidomide analog MGD that reprograms CRBN by inducing a CRBN/MGD neosurface for WIZ engagement to trigger its ubiquitination and degradation by the proteasome.[15] The corresponding complex structure has been solved (PDB: 8TZX). We observed that the current cofolding methods are capable of accurately modeling both the PPI interface and the pocket−ligand interactions within this complex, successfully

https://doi.org/10.1021/acs.jcim.5c01860
J. Chem. Inf. Model. XXXX, XXX, XXX−XXX

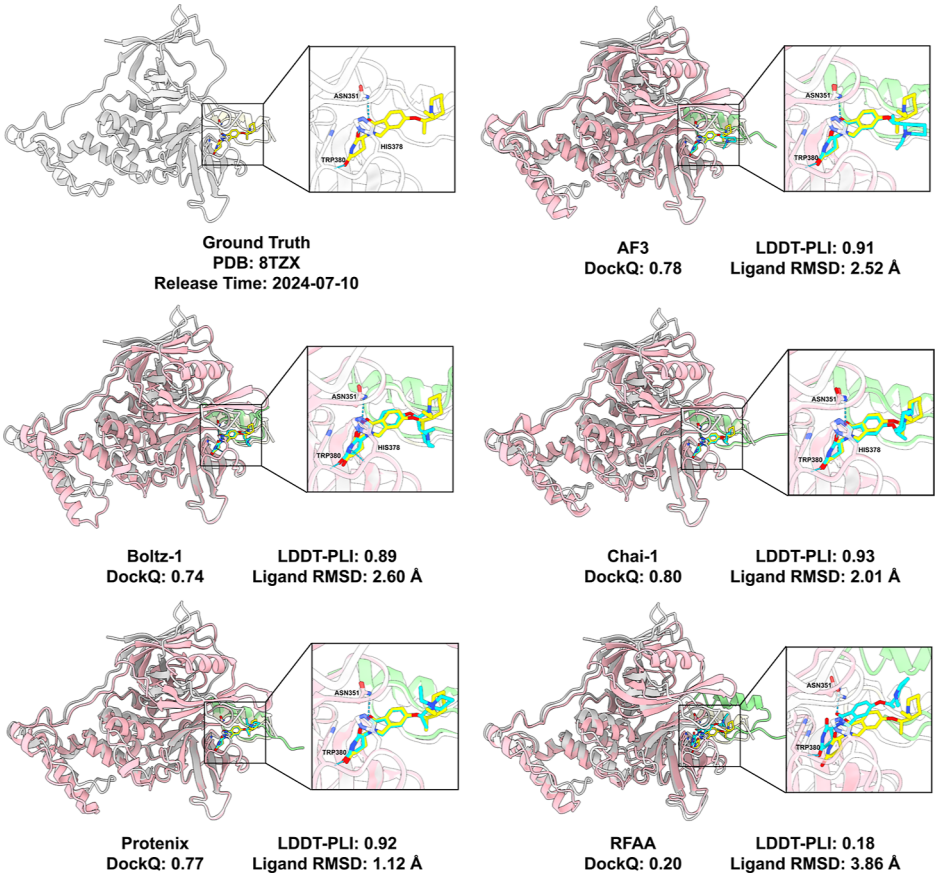

Figure 5. Structural modeling of the CRBN:dWIZ-1:WIZ(ZF7) ternary complex (PDB: 8TZX). The original crystal structure (top left) and computational models generated by five different cofolding methods are shown with their corresponding evaluation metrics. The models are superimposed on the crystal structure based on the dWIZ-1-binding pocket. Proteins are shown in cartoon representation: WIZ(ZF7) is light yellow and CRBN is light gray in the crystal structure, versus light green and light pink, respectively, in the computational models. dWIZ-1 is depicted as yellow sticks (crystal structure) or cyan sticks (models), with key interacting protein residues displayed. Close-up views focus on dWIZ-1 and the interacting residues, with labels indicating residue names and hydrogen bonds shown as blue dotted lines.

recovering most (AF3, Protenix, and RFAA) or all (Boltz-1 and Chai-1) of the key hydrogen bonds between dWIZ-1 and the proteins (Figure 5). It is predictable as WIZ belongs to the Cys2-His2 (C2H2) subfamily, some of which are well-investigated zinc finger substrates targeted by CRBN−MGD complexes.[73] Although WIZ exhibits limited primary sequence similarity (<40% identity) to known thalidomide analogs targeting C2H2 zinc fingers in our homology analysis, the structural conservation of the characteristic G-loop motif among C2H2-type zinc fingers enables specific recognition and binding by CRBN−MGD complexes.[74] Ternary structures of CRBN with different C2H2-type neosubstrate-small-molecule pairs in the training set, such as CK1a−lenalidomide (5FQD), GSPT1−CC885 (5HXB), ZNF692−pomalidomide (6H0G), SALL4−thalidomide (6UML), and IKZF2−ALV1 (7LPS), can promote cofolding methods to capture the inherent binding pattern mediated by the structurally conserved degron motif. As a motif alignment analysis from Monte Rosa Therapeutics predicts that there are 2550 putative G-loop-containing proteins in the human proteome,[74,75] the successful case demonstrates that current cofolding methods could be a promising tool for accurate modeling of G-loop-containing neosubstrates engaged with CRBN−thalidomide-analog complexes.

Given that the preceding case is limited to CRBN-mediated TPD, we sought to explore whether these methods could successfully model ternary complexes involving a broader range of E3 ligases and substrates. UM171 functions as MG, inducing high-affinity interactions between KBTBD4, a substrate receptor of the CUL3−RING E3 ubiquitin ligase complex, and histone deacetylase HDAC1/2, thereby promoting the degradation of the LSD1−CoREST corepressor complex and consequently enhancing *ex vivo* human hematopoietic stem cell self-renewal.[76] We performed a reconstruction of the KBTBD4:UM171:HDAC1 ternary complex (PDB: 8VOJ), a structure included in the MGBench low-homology set. We observed that all methods exhibited poor performance in predicting the PPI interface, protein−ligand interactions, and MG conformation (Figure 6). Notably, the MG predicted by Protenix was not located within the PPI interface, and the structure predicted by RFAA displayed geometrically overlapping chains. We observed that all models correctly identified the HDAC1 binding pocket, likely due to exposure to binary HDAC1−inhibitor complexes in their training data (e.g., PDB: 5ICN).[77] However, they all incorrectly modeled UM171 deep within the pocket, mimicking a conventional inhibitor. This contradicts the experimental structure, where UM171 acts as a cooperative bridge requiring KBTBD4 for engagement, rather than a direct binder.[76] This indicates that the cofolding models failed to capture the ternary cooperativity, instead defaulting to a more familiar binary binding paradigm, likely due to a lack of relevant training data. Furthermore, among the remaining four

https://doi.org/10.1021/acs.jcim.5c01860
J. Chem. Inf. Model. XXXX, XXX, XXX−XXX

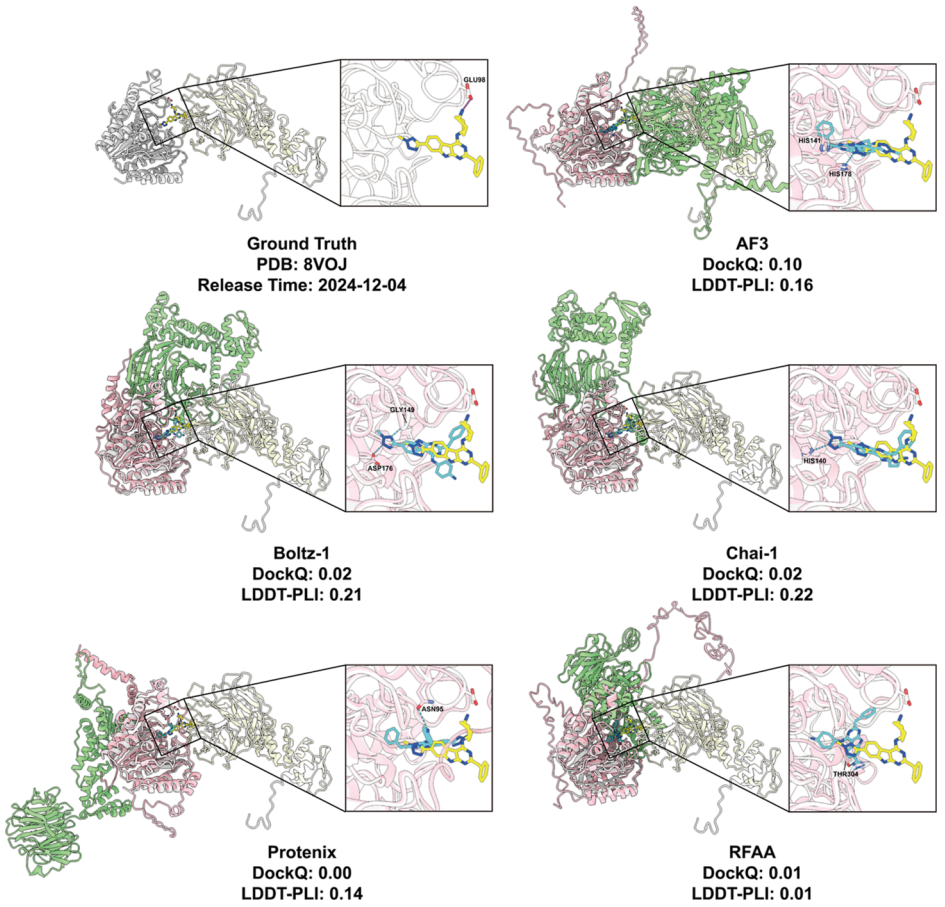

Figure 6. Structural modeling of the KBTBD4:UM171:HDAC1 ternary complex (PDB: 8VOJ). The original crystal structure (top left) and computational models generated by five different cofolding methods are shown with their corresponding evaluation metrics. The models are superimposed on the crystal structure based on the HDAC1 chain. Proteins are shown in cartoon representation: KBTBD4 is light yellow and HDAC1 is light gray in the crystal structure, versus light green and light pink, respectively, in the computational models. UM171 is depicted as yellow sticks (crystal structure) or cyan sticks (models), with key interacting protein residues displayed. Close-up views focus on UM171 and the interacting residues (KBTBD4 is hidden), with labels indicating residue names, hydrogen bonds shown as blue dotted lines, and salt bridges shown as magenta dotted lines.

cases with novel E3 ligases, including DCAF16 and VHL, almost none of the cofolding approaches yielded high-quality ternary complex structures (Table S4). To enhance cofolding performance for other E3 ligases, substantial improvements are still needed in future work.

DISCUSSION

MGs have garnered significant attention due to their favorable druggability and unique MOA.[5] Traditional discovery approaches primarily rely on serendipitous findings and large-scale experimental screening. The structural basis provided by MG ternary complexes is pivotal for mechanistic studies, structure-based virtual screening, *de novo* design, and lead optimization. Emerging AI cofolding methods[43−47] enable *de novo* prediction of these complexes from sequence and chemical data, overcoming limitations of conventional approaches[39−41] in modeling MG-induced conformational changes. However, the modeling capabilities of these methods on MG-engaged ternary complexes remain unclear. Our study systematically assesses the performance and generalization ability of cofolding methods for a possible shift to the next-generation MG discovery paradigm.

Previous collections of MG-engaged ternary complex structures were limited to fewer than 100 entries,[56] which is insufficient for comprehensive evaluation, and most of them were used to train current cofolding methods. We systematically collected a data set containing 221 experimentally determined noncovalent MG-engaged ternary complex structures, named MG-PDB, and conducted benchmarking study over five cofolding methods in our newly introduced benchmark set, named MGBench. Multiple quality assessment metrics were calculated, including DockQ, LDDT-PLI, and ligand RMSD. Overall, all methods demonstrated limited reconstruction capability for MGBench structures, with approximately a 50% success rate for PPI interfaces and ∼30% native interaction recovery rate. Specifically, RFAA failed to predict any structures successfully, whereas AF3-like methods consistently generated reliable models. AF3 exhibited superior performance across all evaluation metrics, demonstrating its SOTA performance. Further key impact analysis showed that performance decoy was observed in larger MGs, gluable PPI with large BSA and domain−domain-type PPI. The benchmark results revealed that current methods remain unable to generalize predictions for novel ternary complexes, failing to adequately capture intricate molecular interaction patterns. These findings aligned with the recent AF3 benchmark study in protein−ligand cofolding,[49] collectively

https://doi.org/10.1021/acs.jcim.5c01860
J. Chem. Inf. Model. XXXX, XXX, XXX−XXX

highlighting fundamental gaps and memorization issue in accurate modeling of protein−ligand complex structures.

The primary obstacle preventing current cofolding methods from accurately predicting MG-bound ternary complex structures stems from severe data scarcity. The PDB contains dramatically fewer "protein−small molecule−protein" interaction entries compared to abundant PPI data.[78] Consequently, these methods, trained on minimal MG−PPI examples, inevitably fail. Furthermore, their AlphaFold-like architectures heavily rely on coevolutionary information encoded in multiple sequence alignments to guide PPI modeling,[44,48,79] while some MG−PPIs lack such intrinsic evolutionary constraints since MGs typically induce neomorphic PPIs. Notably, existing successful MG design cases predominantly target systems with inherent coevolutionary relationships, primarily thalidomide-analog MGDs targeting CRBN-G-loop degrons[74,80] and 14−3−3/client protein stabilizers,[81] where weak endogenous PPIs and biological function upon binding pre-exist.[38] This aligns with our benchmark results showing superior performance on domain−motif-type PPIs and certain MGD targets as these systems retain evolutionarily coupled interaction signatures.

Beyond high-accuracy ternary complex modeling, developing scoring functions to evaluate the binding affinity or degradation efficiency is urgent for computational MG screening. While AI-based scoring function remains impractical due to data scarcity, hybrid physical/AI approaches, such as GlueMap[82] and MOLDE,[83] which integrate molecular dynamics simulations, binding free-energy calculations, and generative AI, have shown promising performance in retrospective validations. An alternative strategy leverages interaction data to train classifiers, exemplified by MaSIF-neosurf's innovative use of biomolecular surface patches to predict binding propensity in ternary systems.[84] However, this approach requires *a priori* strong affinity and stable binding poses between the MG and at least one protein partner, effectively reducing the ternary problem to binary interaction prediction between protein−ligand neosurfaces and protein surfaces, a simplification that limits generalizability. Notably, the confidence scores output by AF3-like models warrant investigation as potential affinity proxies, representing an attractive avenue for future exploration given their intrinsic structural insights.

Despite these challenges, a divide-and-conquer approach leveraging AF3 remains viable. For CRBN-G-loop systems, AF3 reliably generates structural models that can accelerate the discovery of novel MGDs. However, targeting alternative E3 ligases or developing MGDs with distinct MOAs will require systematic accumulation of experimental data and deeper mechanistic studies. A critical open question is whether other E3 ligases exhibit conserved degron-recognition motifs analogous to the CRBN-G-loop interaction pattern. Through the iterative integration of experimental data and conserved interaction constraints, continuously refined AF3 models will emerge as a transformative tool for both MG discovery and mechanistic elucidation.

Overall, while AI biomolecular cofolding methods have advanced MG-engaged ternary complex structure prediction, our benchmark study reveals their limitations and provides important references for future method optimization and rational MG design, thereby advancing computation-driven next-generation MG discovery paradigms.

■ ASSOCIATED CONTENT

Data Availability Statement

Code for reproducing the analysis and plots presented in this paper is available at https://github.com/yiyanliao/MGBench. The input JSON files and experimental structure mmCIF files are available at 10.5281/zenodo.16938658. The PDB IDs and detailed information on MG-PDB and MGBench are listed in the Supporting Information (XLSX file).

Supporting Information

The Supporting Information is available free of charge at https://pubs.acs.org/doi/10.1021/acs.jcim.5c01860.

Cofolding methods (Supporting Information Methods); overall metrics distributions of structural modeling for resolution-filtered MG-PDB data set; relationship between evaluation metrics and interacting mode; relationship between evaluation metrics and MG type; summary of data set information; counts of successfully reconstructed MG ternary complexes among cofolding methods; summary of domain−motif structures in resolution-filtered MG-PDB and MGBench; metrics of novel E3 ligase ternary complexes; and ligand RMSD of the KBTBD4:UM171:HDAC1 ternary complex (8VOJ) using pocket-based and chain-based alignments (PDF)

Detailed information on the MG-PDB (XLSX)

■ AUTHOR INFORMATION

Corresponding Authors

Jintao Zhu − *Center for Quantitative Biology, Academy for Advanced Interdisciplinary Studies, Peking University, Beijing 100871, China*; Email: zhujt@stu.pku.edu.cn.

Luhua Lai − *Center for Quantitative Biology, Academy for Advanced Interdisciplinary Studies, Peking University, Beijing 100871, China; BNLMS, College of Chemistry and Molecular Engineering and Peking-Tsinghua Center for Life Sciences, Academy for Advanced Interdisciplinary Studies, Peking University, Beijing 100871, China; Peking University Chengdu Academy for Advanced Interdisciplinary Biotechnologies, Chengdu, Sichuan 610213, China;* orcid.org/0000-0002-8343-7587; Email: lhlai@pku.edu.cn

Jianfeng Pei − *Center for Quantitative Biology, Academy for Advanced Interdisciplinary Studies, Peking University, Beijing 100871, China;* orcid.org/0000-0002-8482-1185; Email: jfpei@pku.edu.cn

Authors

Yiyan Liao − *School of Life Sciences, Peking University, Beijing 100871, China*

Juan Xie − *BNLMS, College of Chemistry and Molecular Engineering, Peking University, Beijing 100871, China;* orcid.org/0000-0001-6975-0449

Complete contact information is available at: https://pubs.acs.org/10.1021/acs.jcim.5c01860

Author Contributions

#Y.L. and J.Z. have contributed equally. J.Z. designed the research. Y.L. and J.Z. collected the benchmark set. Y.L. conducted the experiments and analyzed the data. Y.L., J.Z., and J.X. discussed the results. Y.L. and J.Z. wrote the manuscript. J.P., L.L., and J.Z. supervised the project. J.P., L.L., and J.X. revised the manuscript. All authors read and approved the final manuscript.

https://doi.org/10.1021/acs.jcim.5c01860
J. Chem. Inf. Model. XXXX, XXX, XXX−XXX

Notes

The authors declare no competing financial interest.

■ ACKNOWLEDGMENTS

This work has been supported in part by the National Natural Science Foundation of China (22033001 and T2321001), the National Key R&D Program of China (2023YFF1205103), the Chinese Academy of Medical Sciences (2021-I2M-5-014), the Anhui's Plans for Major Provincial Science & Technology Projects (202303a07020009), and the Beijing Natural Science Foundation (QY25135). We thank the Computing Platform of the Center for Life Science (Peking University) for providing resources for the GPU-based model inference. Part of the computation was performed on the computing platform of the Infinite Intelligence Pharma Ltd.

■ REFERENCES

(1) Glasgow, A. A.; et al. Computational design of a modular protein sense-response system. *Science* **2019**, *366*, 1024−1028.
(2) Zhao, L.; Zhao, J.; Zhong, K.; Tong, A.; Jia, D. Targeted protein degradation: mechanisms, strategies and application. *Signal Transduction Targeted Ther.* **2022**, *7*, 113.
(3) Zhong, G.; Chang, X.; Xie, W.; Zhou, X. Targeted protein degradation: advances in drug discovery and clinical practice. *Signal Transduction Targeted Ther.* **2024**, *9*, 308.
(4) Krönke, J.; et al. Lenalidomide causes selective degradation of IKZF1 and IKZF3 in multiple myeloma cells. *Science* **2014**, *343*, 301−305.
(5) Schreiber, S. L. The rise of molecular glues. *Cell* **2021**, *184*, 3−9.
(6) Liu, J.; et al. Calcineurin is a common target of cyclophilin-cyclosporin A and FKBP-FK506 complexes. *Cell* **1991**, *66*, 807−815.
(7) Schreiber, S. L.; Crabtree, G. R. The mechanism of action of cyclosporin A and FK506. *Immunol. Today* **1992**, *13*, 136−142.
(8) Haggarty, S. J.; et al. Dissecting cellular processes using small molecules: identification of colchicine-like, taxol-like and other small molecules that perturb mitosis. *Chem. Biol.* **2000**, *7*, 275−286.
(9) Chamberlain, P. P.; Cathers, B. E. Cereblon modulators: Low molecular weight inducers of protein degradation. *Drug Discovery Today: Technol.* **2019**, *31*, 29−34.
(10) Sasso, J. M.; et al. Molecular glues: The adhesive connecting targeted protein degradation to the clinic. *Biochemistry* **2023**, *62*, 601−623.
(11) Geiger, T. M.; Schäfer, S. C.; Dreizler, J. K.; Walz, M.; Hausch, F. Clues to molecular glues. *Curr. Res. Chem. Biol.* **2022**, *2*, 100018.
(12) Domostegui, A.; Nieto-Barrado, L.; Perez-Lopez, C.; Mayor-Ruiz, C. Chasing molecular glue degraders: screening approaches. *Chem. Soc. Rev.* **2022**, *51*, 5498−5517.
(13) Dewey, J. A.; et al. Molecular glue discovery: current and future approaches. *J. Med. Chem.* **2023**, *66*, 9278−9296.
(14) Henley, M. J.; Koehler, A. N. Advances in targeting 'undruggable' transcription factors with small molecules. *Nat. Rev. Drug Discovery* **2021**, *20*, 669−688.
(15) Ting, P. Y.; et al. A molecular glue degrader of the WIZ transcription factor for fetal hemoglobin induction. *Science* **2024**, *385*, 91−99.
(16) Oberheide, A.; et al. Site-specific molecular glues for the 14−3-3/Tau pS214 protein−protein interaction via reversible covalent imine tethering. *RSC Med. Chem.* **2025**, *16*, 2190−2201.
(17) Konstantinidou, M.; Arkin, M. R. Molecular glues for protein-protein interactions: progressing toward a new dream. *Cell Chem. Biol.* **2024**, *31*, 1064−1088.
(18) Wang, B.; Cao, S.; Zheng, N. Emerging strategies for prospective discovery of molecular glue degraders. *Curr. Opin. Struct. Biol.* **2024**, *86*, 102811.
(19) Teng, M.; Gray, N. S. The rise of degrader drugs. *Cell Chem. Biol.* **2023**, *30*, 864−878.
(20) Chen, S.; Zacharias, M. What makes a good protein−protein interaction stabilizer: analysis and application of the dual-binding mechanism. *ACS Cent. Sci.* **2023**, *9*, 969−979.
(21) Zhu, J.; Lai, L.; Pei, J. Toward *in silico* design of protein-protein interaction stabilizers. *ACS Cent. Sci.* **2023**, *9*, 861−863.
(22) Dang, D. T. Molecular approaches to protein dimerization: opportunities for supramolecular chemistry. *Front. Chem.* **2022**, *10*, 829312.
(23) Wang, T.; et al. Discovery of small-molecule inhibitors of the PD-1/PD-L1 axis that promote PD-L1 internalization and degradation. *J. Med. Chem.* **2022**, *65*, 3879−3893.
(24) Lipinski, C. A.; Lombardo, F.; Dominy, B. W.; Feeney, P. J. Experimental and computational approaches to estimate solubility and permeability in drug discovery and development settings. *Adv. Drug Delivery Rev.* **2001**, *46*, 3−26.
(25) Zheng, S.; et al. Accelerated rational PROTAC design via deep learning and molecular simulations. *Nat. Mach. Intell.* **2022**, *4*, 739−748.
(26) Li, B.; Ran, T.; Chen, H. 3D based generative PROTAC linker design with reinforcement learning. *Briefings Bioinf.* **2023**, *24*, bbad323.
(27) Drummond, M. L.; Williams, C. I. *In silico* modeling of PROTAC-mediated ternary complexes: Validation and application. *J. Chem. Inf. Model.* **2019**, *59*, 1634−1644.
(28) Zaidman, D.; Prilusky, J.; London, N. PRosettaC: Rosetta based modeling of PROTAC mediated ternary complexes. *J. Chem. Inf. Model.* **2020**, *60*, 4894−4903.
(29) Sakamoto, K. M.; et al. Protacs: chimeric molecules that target proteins to the Skp1-Cullin-F box complex for ubiquitination and degradation. *Proc. Natl. Acad. Sci. U.S.A.* **2001**, *98*, 8554−8559.
(30) Bemis, T. A.; La Clair, J. J.; Burkart, M. D. Unraveling the role of linker design in proteolysis targeting chimeras. *J. Med. Chem.* **2021**, *64*, 8042−8052.
(31) Dong, G.; Ding, Y.; He, S.; Sheng, C. Molecular glues for targeted protein degradation: from serendipity to rational discovery. *J. Med. Chem.* **2021**, *64*, 10606−10620.
(32) Ito, T.; et al. Identification of a primary target of thalidomide teratogenicity. *Science* **2010**, *327*, 1345−1350.
(33) Chamberlain, P. P.; et al. Structure of the human Cereblon-DDB1-lenalidomide complex reveals basis for responsiveness to thalidomide analogs. *Nat. Struct. Mol. Biol.* **2014**, *21*, 803−809.
(34) Fischer, E. S.; et al. Structure of the DDB1-CRBN E3 ubiquitin ligase in complex with thalidomide. *Nature* **2014**, *512*, 49−53.
(35) Mayor-Ruiz, C.; et al. Rational discovery of molecular glue degraders via scalable chemical profiling. *Nat. Chem. Biol.* **2020**, *16*, 1199−1207.
(36) Graves, B.; et al. Activation of the p53 pathway by small-molecule-induced MDM2 and MDMX dimerization. *Proc. Natl. Acad. Sci. U.S.A.* **2012**, *109*, 11788−11793.
(37) Hemant Kumar, S.; Venkatachalapathy, M.; Sistla, R.; Poongavanam, V. Advances in molecular glues: exploring chemical space and design principles for targeted protein degradation. *Drug Discovery Today* **2024**, *29*, 104205.
(38) Cao, S.; et al. Defining molecular glues with a dual-nanobody cannabidiol sensor. *Nat. Commun.* **2022**, *13*, 815.
(39) Miller, E. B.; et al. Reliable and accurate solution to the induced fit docking problem for protein−ligand binding. *J. Chem. Theory Comput.* **2021**, *17*, 2630−2639.
(40) Zhu, J.; Gu, Z.; Pei, J.; Lai, L. DiffBindFR: an SE (3) equivariant network for flexible protein−ligand docking. *Chem. Sci.* **2024**, *15*, 7926−7942.
(41) Lu, W.; et al. DynamicBind: predicting ligand-specific protein-ligand complex structure with a deep equivariant generative model. *Nat. Commun.* **2024**, *15*, 1071.
(42) Karamanos, T. K. Chasing long-range evolutionary couplings in the AlphaFold era. *Biopolymers* **2023**, *114*, No. e23530.
(43) Krishna, R.; et al. Generalized biomolecular modeling and design with RoseTTAFold All-Atom. *Science* **2024**, *384*, No. eadl2528.

https://doi.org/10.1021/acs.jcim.5c01860
J. Chem. Inf. Model. XXXX, XXX, XXX−XXX

(44) Abramson, J.; et al. Accurate structure prediction of biomolecular interactions with AlphaFold 3. *Nature* **2024**, *630*, 493−500.
(45) Boitreaud, J.; Dent, J.; McPartlon, M.; Meier, J.; Reis, V.; Rogozhnikov, A.; Wu, K. Chai-1: decoding the molecular interactions of life. *bioRxiv* **2024**, 615955.
(46) Wohlwend, J.; Corso, G.; Passaro, S.; Getz, N.; Reveiz, M.; Leidal, K.; Swiderski, W.; Atkinson, L.; Portnoi, T.; Chinn, I.; et al. Boltz-1 democratizing biomolecular interaction modeling. *bioRxiv* **2024**, 624167.
(47) Chen, X.; Zhang, Y.; Lu, C.; Ma, W.; Guan, J.; Gong, C.; Yang, J.; Zhang, H.; Zhang, K.; Wu, S.; et al. Protenix - advancing structure prediction through a comprehensive AlphaFold3 reproduction. *bioRxiv* **2025**, 631967.
(48) Jumper, J.; et al. Highly accurate protein structure prediction with AlphaFold. *Nature* **2021**, *596*, 583−589.
(49) Škrinjar, P.; Eberhardt, J.; Durairaj, J.; Schwede, T. Have protein-ligand co-folding methods moved beyond memorisation? *bioRxiv* **2025**, 636309.
(50) Wee, J.; Wei, G. Evaluation of AlphaFold 3's protein−protein complexes for predicting binding free energy changes upon mutation. *J. Chem. Inf. Model.* **2024**, *64*, 6676−6683.
(51) He, X.; Li, J.; Shen, S.; Xu, H. E. Alphafold3 versus experimental structures: assessment of the accuracy in ligand-bound G protein-coupled receptors. *Acta Pharmacol. Sin.* **2025**, *46*, 1111−1122.
(52) Dunlop, N.; Erazo, F.; Jalalypour, F.; Mercado, R. Predicting PROTAC-mediated ternary complexes with AlphaFold3 and Boltz-1. *ChemRxiv* **2025**, gfd6c-v2.
(53) Berman, H. M.; et al. The Protein Data Bank. *Nucleic Acids Res.* **2000**, *28*, 235−242.
(54) Burley, S. K.; et al. Updated resources for exploring experimentally-determined PDB structures and Computed Structure Models at the RCSB Protein Data Bank. *Nucleic Acids Res.* **2025**, *53*, D564−D574.
(55) Rose, Y.; et al. RCSB Protein Data Bank: Architectural advances towards integrated searching and efficient access to macromolecular structure data from the PDB archive. *J. Mol. Biol.* **2021**, *433*, 166704.
(56) Rui, H.; Ashton, K. S.; Min, J.; Wang, C.; Potts, P. R. Protein-protein interfaces in molecular glue-induced ternary complexes: classification, characterization, and prediction. *RSC Chem. Biol.* **2023**, *4*, 192−215.
(57) Steinegger, M.; Söding, J. MMseqs2 enables sensitive protein sequence searching for the analysis of massive data sets. *Nat. Biotechnol.* **2017**, *35*, 1026−1028.
(58) Flachsenberg, F.; Ehrt, C.; Gutermuth, T.; Rarey, M. Redocking the PDB. *J. Chem. Inf. Model.* **2024**, *64*, 219−237.
(59) Meyder, A.; et al. StructureProfiler: an all-in-one tool for 3D protein structure profiling. *Bioinformatics* **2019**, *35*, 874−876.
(60) Cruickshank, D. W. Remarks about protein structure precision. *Acta Crystallogr., Sect. D:Biol. Crystallogr.* **1999**, *55*, 583−601.
(61) Smart, O. S.; et al. Validation of ligands in macromolecular structures determined by X-ray crystallography. *Acta Crystallogr., Sect. D:Struct. Biol.* **2018**, *74*, 228−236.
(62) Meng, E. C.; et al. UCSF ChimeraX: tools for structure building and analysis. *Protein Sci.* **2023**, *32*, No. e4792.
(63) Mirabello, C.; Wallner, B. DockQ v2: improved automatic quality measure for protein multimers, nucleic acids, and small molecules. *Bioinformatics* **2024**, *40*, btae586.
(64) Robin, X.; et al. Assessment of protein-ligand complexes in CASP15. *Proteins: Struct., Funct., Bioinf.* **2023**, *91*, 1811−1821.
(65) Biasini, M.; et al. OpenStructure: an integrated software framework for computational structural biology. *Acta Crystallogr., Sect. D:Biol. Crystallogr.* **2013**, *69*, 701−709.
(66) Chakravarty, D.; Guharoy, M.; Robert, C. H.; Chakrabarti, P.; Janin, J. Reassessing buried surface areas in protein-protein complexes. *Protein Sci.* **2013**, *22*, 1453−1457.
(67) Eshak, F.; Goupil-Lamy, A. Advancements in nanobody epitope prediction: a comparative study of AlphaFold2Multimer vs AlphaFold3. *J. Chem. Inf. Model.* **2025**, *65*, 1782−1797.
(68) Basu, S.; Wallner, B. DockQ: A quality measure for protein-protein docking models. *PLoS One* **2016**, *11*, No. e0161879.
(69) Jin, X.; et al. Natural products used as a chemical library for protein-protein interaction targeted drug discovery. *J. Mol. Graphics Modell.* **2018**, *79*, 46−58.
(70) Yin, L.; et al. Research advancements in molecular glues derived from natural product scaffolds: chemistry, targets, and molecular mechanisms. *Chin. Herb. Med.* **2025**, *17*, 235−245.
(71) Justice, M.; Carico, Z. M.; Stefan, H. C.; Dowen, J. M. A WIZ/Cohesin/CTCF complex anchors DNA loops to define gene expression and cell identity. *Cell Rep.* **2020**, *31*, 107503.
(72) Justice, M.; Bryan, A. F.; Limas, J. C.; Cook, J. G.; Dowen, J. M. Chromosomal localization of cohesin is differentially regulated by WIZ, WAPL, and G9a. *BMC Genomics* **2022**, *23*, 337.
(73) Sievers, Q. L.; et al. Defining the human C2H2 zinc finger degrome targeted by thalidomide analogs through CRBN. *Science* **2018**, *362*, No. eaat0572.
(74) Oleinikovas, V.; Gainza, P.; Ryckmans, T.; Fasching, B.; Thomä, N. H. From thalidomide to rational molecular glue design for targeted protein degradation. *Annu. Rev. Pharmacol. Toxicol.* **2024**, *64*, 291−312.
(75) Petzold, G.; et al. Mining the CRBN target space redefines rules for molecular glue−induced neosubstrate recognition. *Science* **2025**, *389*, No. eadt6736.
(76) Yeo, M. J.; et al. UM171 glues asymmetric CRL3−HDAC1/2 assembly to degrade CoREST corepressors. *Nature* **2025**, *639*, 232−240.
(77) Watson, P. J.; et al. Insights into the activation mechanism of class I HDAC complexes by inositol phosphates. *Nat. Commun.* **2016**, *7*, 11262.
(78) Kovtun, D.; Akdel, M.; Goncearenco, A.; Zhou, G.; Holt, G.; Baugher, D.; Lin, D.; Adeshina, Y.; Castiglione, T.; Wang, X.; et al. PINDER: the protein interaction dataset and evaluation resource. *bioRxiv* **2024**, 603980.
(79) Evans, R.; O'Neill, M.; Pritzel, A.; Antropova, N.; Senior, A.; Green, T.; Žídek, A.; Bates, R.; Blackwell, S.; Yim, J.; et al. Protein complex prediction with AlphaFold-Multimer. *bioRxiv* **2021**, 463034.
(80) Kozicka, Z.; Thomä, N. H. Haven't got a glue: protein surface variation for the design of molecular glue degraders. *Cell Chem. Biol.* **2021**, *28*, 1032−1047.
(81) Tian, Y.; et al. Recent developments in 14−3−3 stabilizers for regulating protein−protein interactions: an update. *J. Med. Chem.* **2025**, *68*, 2124−2146.
(82) Izaguirre, J. A.; Wu, Y.; McDargh, Z.; Palpant, T.; Razavi, A. M.; Trovato, F.; Koh, C.; Xu, H. Computational modeling of ternary complex formation and targeted protein degradation mediated by molecular glues. *bioRxiv* **2025**, 632817.
(83) Ben Geoffrey, A.; Agrawal, D.; Kulkarni, N. M.; Gunasekaran, M. Molecular Glue-Design-Evaluator (MOLDE): an advanced method for in-silico molecular glue design. *ACS Omega* **2025**, *10*, 6650−6662.
(84) Marchand, A.; et al. Targeting protein−ligand neosurfaces with a generalizable deep learning tool. *Nature* **2025**, *639*, 522−531.

https://doi.org/10.1021/acs.jcim.5c01860
J. Chem. Inf. Model. XXXX, XXX, XXX−XXX